Supplementary Information

Shear-Aligned Nanocellulose Enabling Stable All-Solid-State Lithium Batteries

Jinping Yu,[a] Guangzeng Cheng,[a] Ziwei Lu,[a] Yonghui Wang,[a] Fanlu Meng*[a] and Jingyi Wu*[a]

[a] School of Materials Science and Engineering, Ocean University of China, Qingdao 266404, China.

E-mail: mengfanlu@ouc.edu.cn; wujingyi@ouc.edu.cn

1. Supplementary Methods

1.1 Material characterization

X-ray diffraction (XRD) measurements of the samples were performed on a Bruker D8 Advance diffractometer with Cu-Kα radiation. The morphology and structure were analyzed using a scanning electron microscope (ZEISS Gemini SEM 300). The Raman spectrum was measured using a Jobin-Yvon Labram HR-800 to characterize the dissociation of lithium salt. The FTIR-Spectrometer (Nicolet iS20) was used to characterize changes in the internal chemical bonds of materials. Differential Scanning Calorimetry (DSC) was used to determine the glass transition temperature and melting temperature of the electrolyte. The Wide-Angle X-ray diffraction (WAXS), is used to provide more intuitive evidence of orientation structure. Thermogravimetric Analysis (TGA) is a technique for analyzing the thermal stability of materials. The X-ray Photoelectron Spectroscopy (XPS) test is conducted using the Thermo Scientific K-Alpha instrument, which can accurately analyze the elemental composition of a material's surface, including the types of elements and their relative concentrations.

1.2 Electrochemical measurements

EIS of electrolyte was obtained using an electrochemical workstation (CHI660E, Chenhua) in the frequency range of 10^{-2} to 7×10^{6} Hz by applying a 5 mV AC oscillation. The test cell was fabricated by sandwiching the electrolyte between two steel plates. The Tafel plot test was conducted by assembling a lithium symmetric cell and scanning from -0.25 V to 0.25 V at a scan rate of 1 mV s^{-1}. LSV curves were examined from the open-circuit voltage to 6 V versus Li/Li^{+} at a scanning rate of 1 mV s^{-1}. Assemble LFP/CPE/Li and Li/CPE/Li batteries and conduct galvanostatic charge/discharge tests on the batteries at 30 °C and 60 °C using a battery test system (LAND CT3002A), with the voltage range from 2.5 to 4 V for LFP full cells. The critical current density (CCD) was evaluated by galvanostatic cycling of Li/CPE/Li symmetric cells at 60 °C, with increasing current densities from 0.1 to 1.3 mA cm^{-2} step by step.

1.3 Ionic conductivity, activation energy, and ionic transference number

The ionic conductivity (σ) of SSEs is calculated by measuring the electrochemical impedance spectroscopy from 30 °C to 80 °C and using the following equation:

$$\sigma = \frac{L}{RS} \tag{1}$$

Where L is the thickness of the electrolyte, S is the area of the stainless steel, and R is the resistance obtained by measuring the EIS of the electrolyte sandwiched between the two stainless steels. The relationship between ionic conductivity and temperature conforms to the Vogel-Tamman-Fulcher (VTF) equation:

$$\sigma = \frac{A}{\sqrt{T}}\exp\left(\frac{-Ea}{K_B(T - T_0)}\right)$$

(2)

Where A is the exponential factor, representing the effective concentration of charge carriers. T is the absolute temperature. T_0 is the ideal glass transition temperature (Vogel temperature). Ea is the activation energy. K_B is Boltzmann's constant, approximately equal to 1.381×10^{-23} J K^{-1}. Therefore, there is a linear relationship between 1000/T and log (σ), where σ represents the ionic conductivity. By plotting 1000/T on the x-axis and log (σ) on the y-axis, a linear fit can be obtained and the slope can be calculated. The slope can then be used to calculate the activation energy.

The lithium-ion transference number (t_{Li^+}) is an important parameter to measure its migration ability in solid-state electrolytes. This parameter can be obtained by assembling a Li/SSEs/Li battery to perform chronoamperometry and AC impedance spectroscopy, followed by calculations using the following equation:

$$t^+ = \frac{I_{ss}(\Delta V - I_0R_0)}{I_0(\Delta V - I_{ss}R_{ss})} \tag{3}$$

ΔV represents a small and constant potential difference applied to the measured symmetric cell, typically around 10 mV. I_0 and I_{ss} are the initial current and steady-state current. R_0 and R_{ss} represent the initial resistance and steady-state resistance.

1.4 Simulation

COMSOL Multiphysics software with lithium battery module was used to simulate Li^+ concentration distributions and potential distributions in O-CPE, R-CPE, and PEO electrolytes. $LiFePO_4$ serves as the active material in the cathode and lithium metal works as the anode. All models employed electrolytes with a thickness of 25 μm. The cells were subjected to constant current charging at a rate of 0.1 C. The ion concentration distribution and potential distribution were analyzed when the cells reached a voltage of 4 V.

2. Supporting Figures and Tables

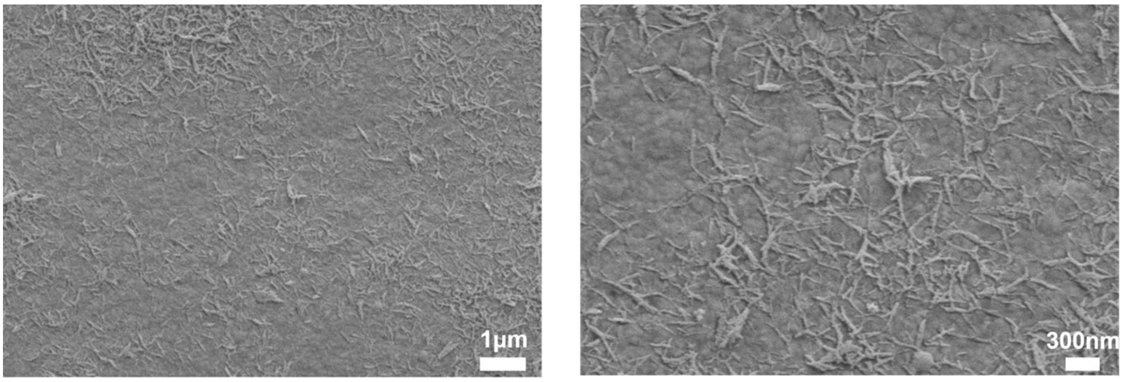

Fig. S1. SEM images of CNCs-Li.

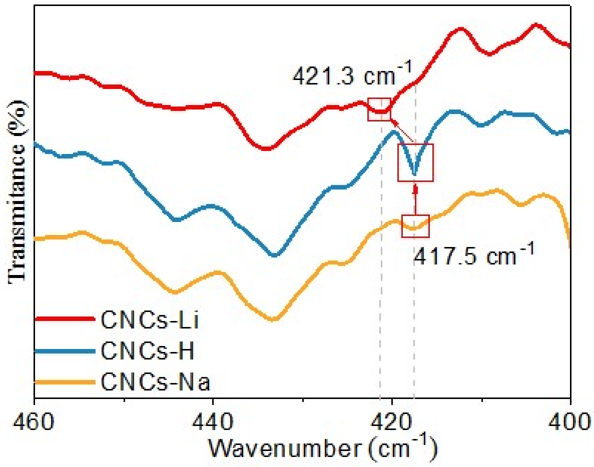

Fig. S2. The magnified view of the FTIR spectra at 460 to 400 cm^{-1} of CNCs-Li, CNCs-Na, and CNCs-H.

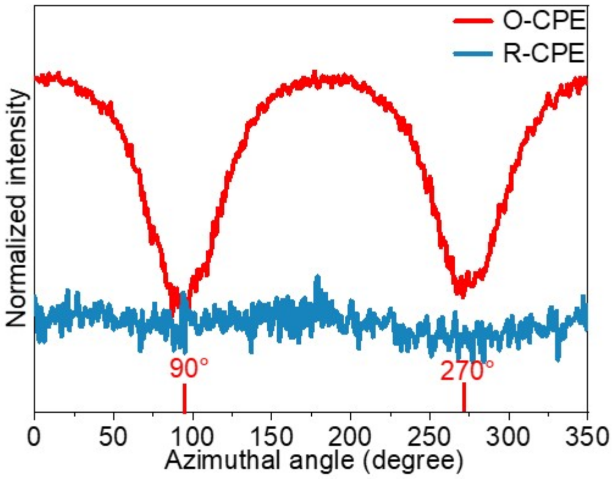

Fig. S3. Azimuthal maps of O-CPE and R-CPE films.

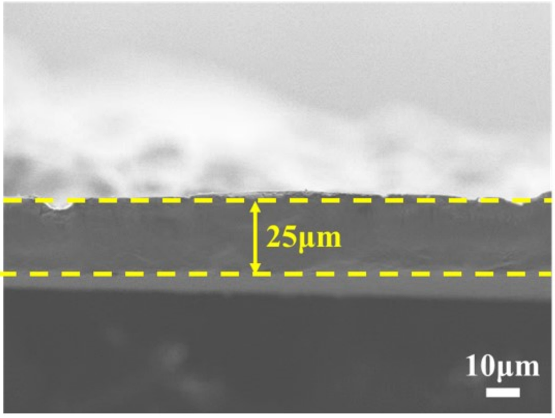

Fig. S4. Thickness measurement of O-CPE films and cross-sectional SEM images.

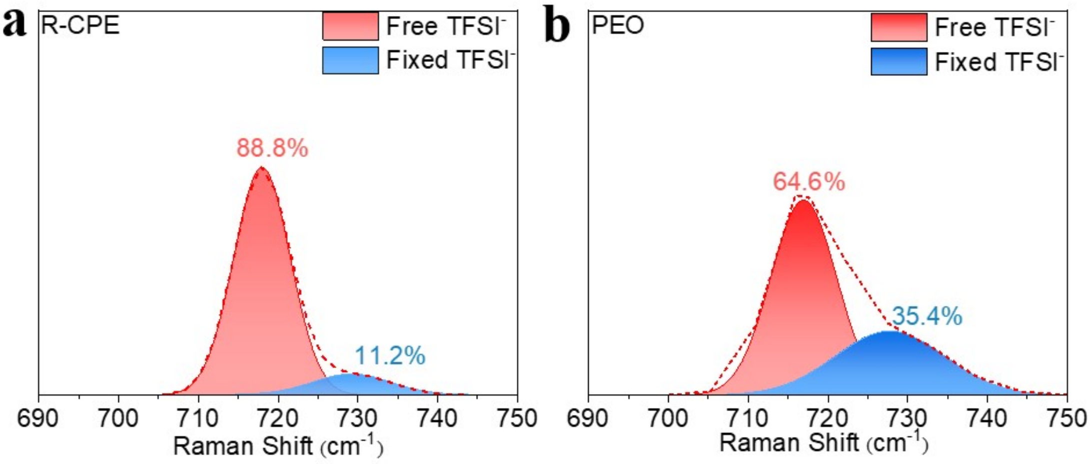

Fig. S5. Raman spectra of (a) R-CPE and (b) PEO films.

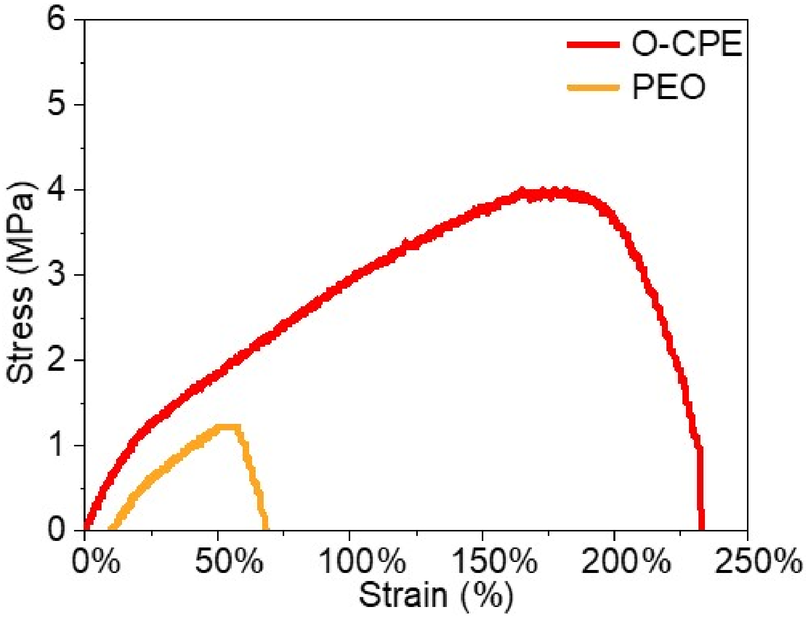

Fig. S6. Stress-strain curves of O-CPE and PEO films.

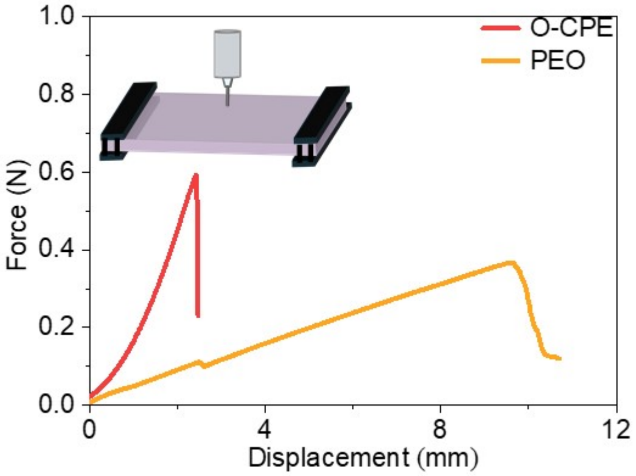

Fig. S7. Puncture curves of O-CPE and PEO films.

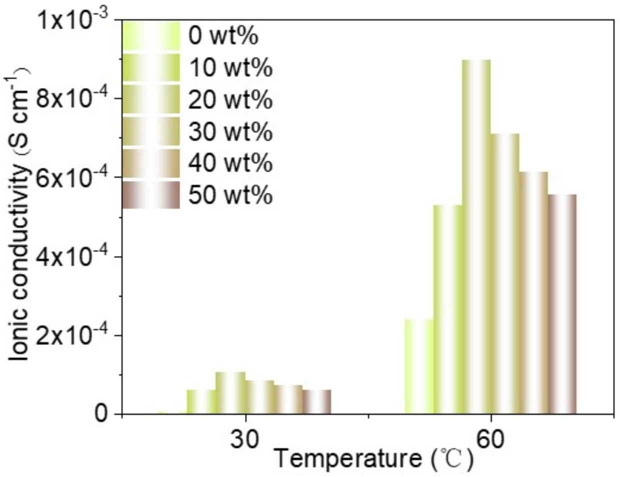

Fig. S8. The ion conductivity of O-CPE with the addition of different amounts of CNCs-Li at different temperatures.

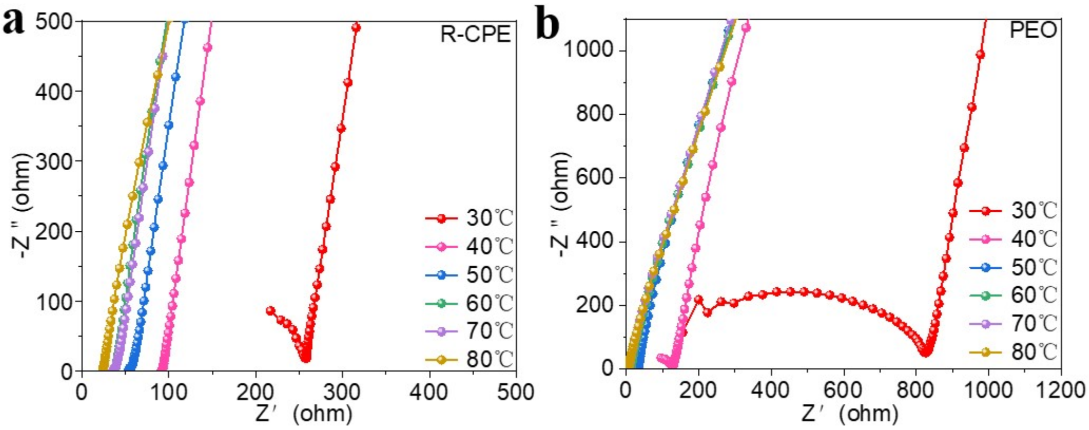

Fig. S9. EIS curves of (a) R-CPE and (b) PEO from 30 to 80 °C.

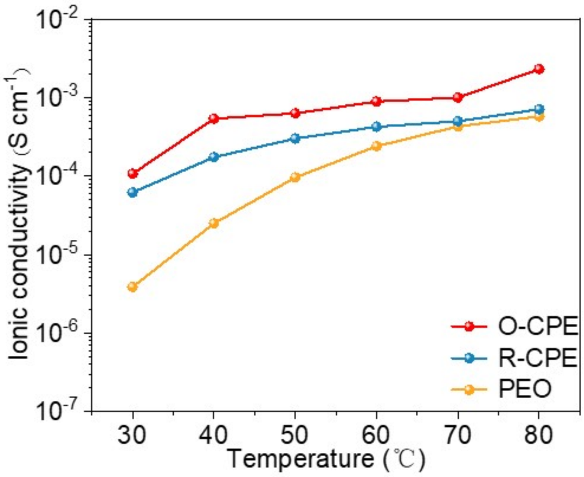

Fig. S10. Ionic conductivity of different electrolyte films from 30 to 80 °C.

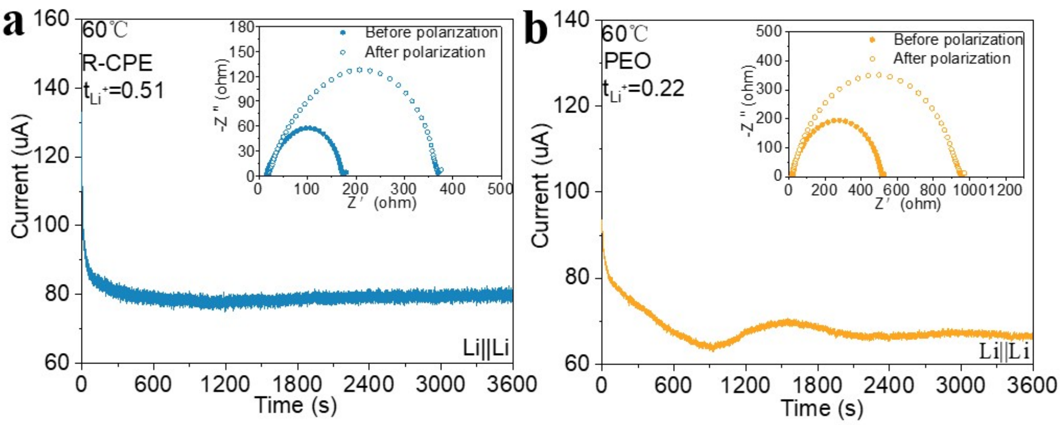

Fig. S11. Current-time curve of (a) R-CPE and (b) PEO Li symmetric cells at 60 °C.

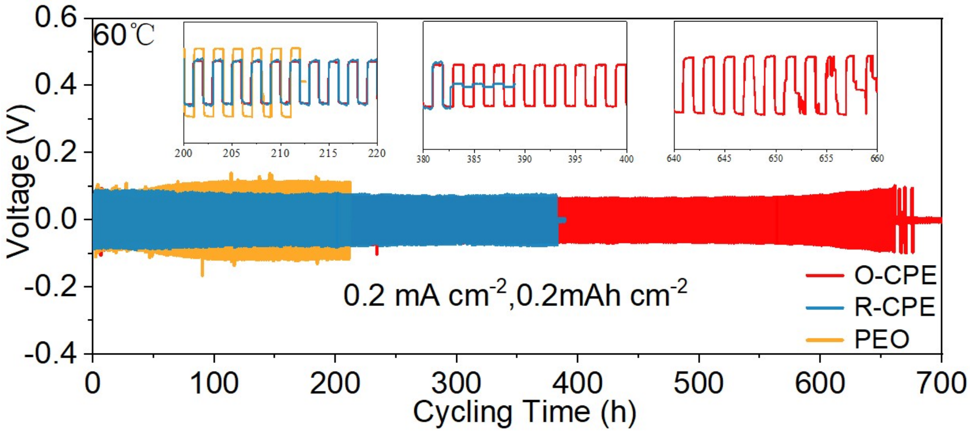

Fig. S12. Long-term cycling of Li/Li symmetric cells with O-CPE, R-CPE, and PEO at 0.2 mA cm^{-2} and 0.2 mAh cm^{-2} and 60 °C.

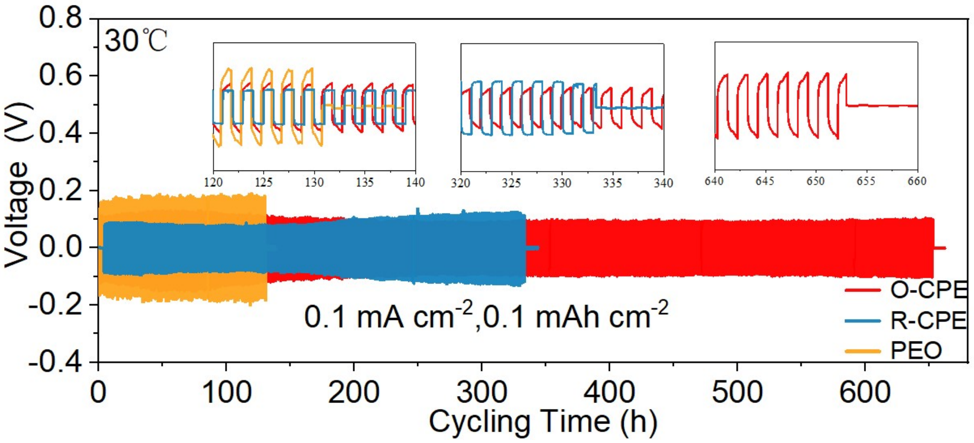

Fig. S13. Long-term cycling of Li/Li symmetric cells with O-CPE, R-CPE, and PEO at 0.1 mA cm^{-2} and 0.1 mAh cm^{-2} and 30 °C.

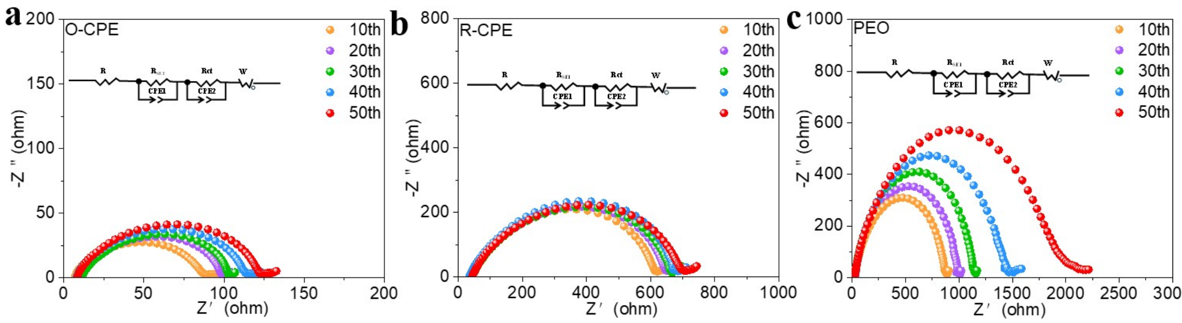

Fig. S14. EIS curves at different cycle numbers of (a) O-CPE, (b) R-CPE, and (c) PEO at 60 °C.

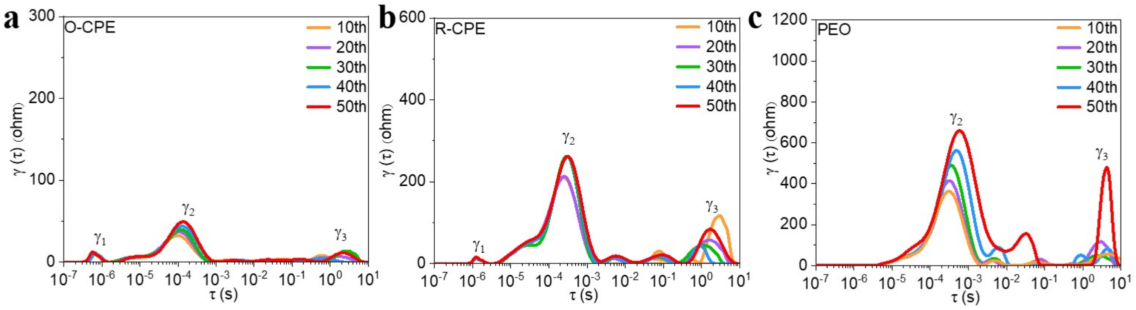

Fig. S15. DRT calculated from EIS at different cycle numbers of (a) O-CPE, (b) R-CPE, and (c) PEO at 60 °C.

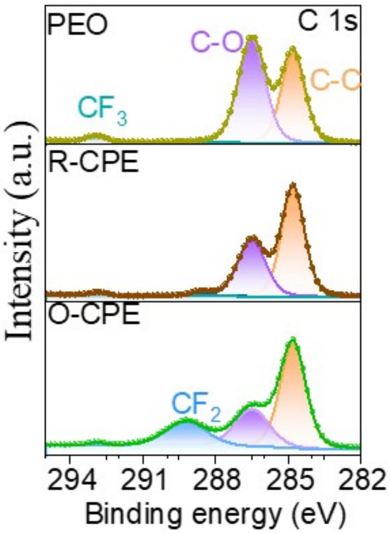

Fig. S16. High-resolution C 1s XPS spectra of Li metal surface after cycling.

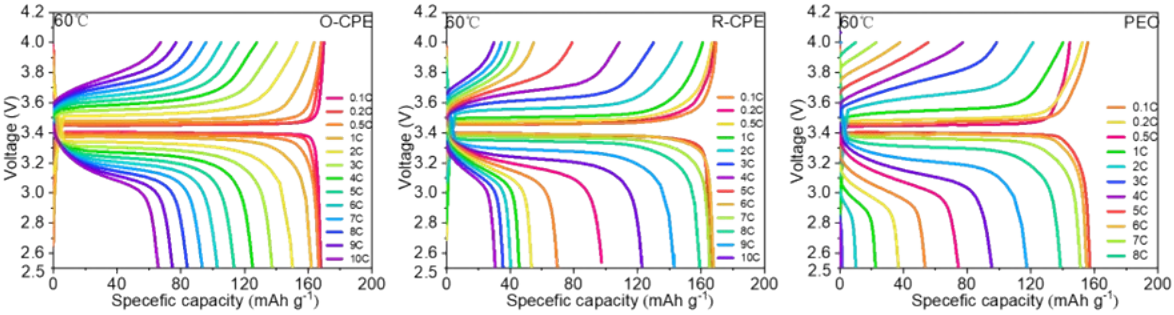

Fig. S17. Corresponding voltage curves of (a) O-CPE, (b) R-CPE and (c) PEO full cells under different rates at 60 °C.

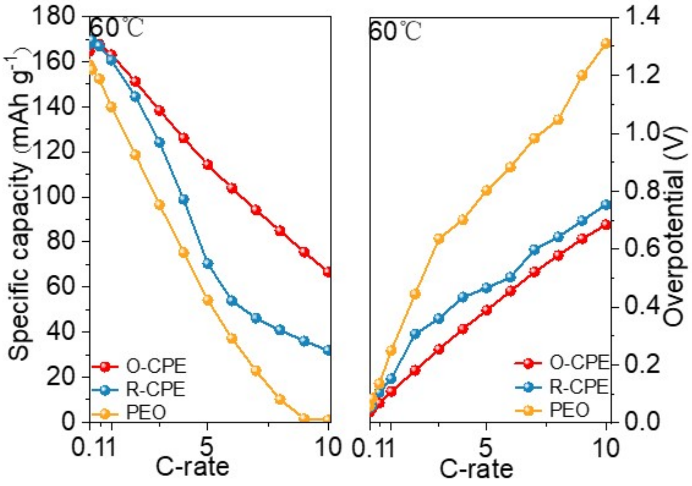

Fig. S18. Overpotentials of different electrolyte films at various rates in LFP-based cells.

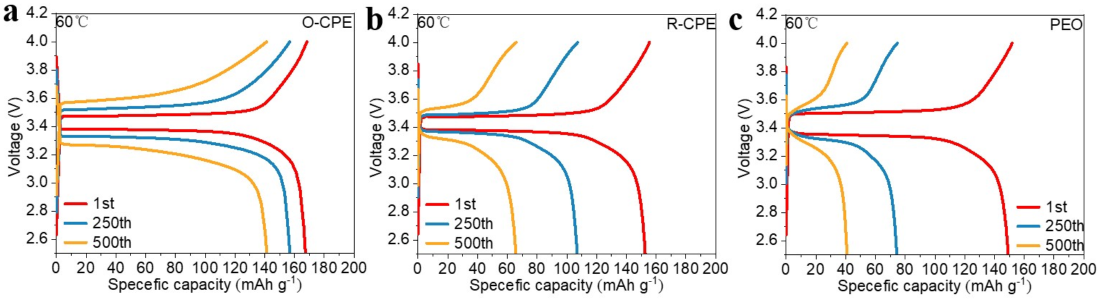

Fig. S19. Corresponding voltage curves of the full cells with (a) O-CPE, (b) R-CPE and (c) PEO at the 1st, 250th and 500th cycles under 1C at 60 °C.

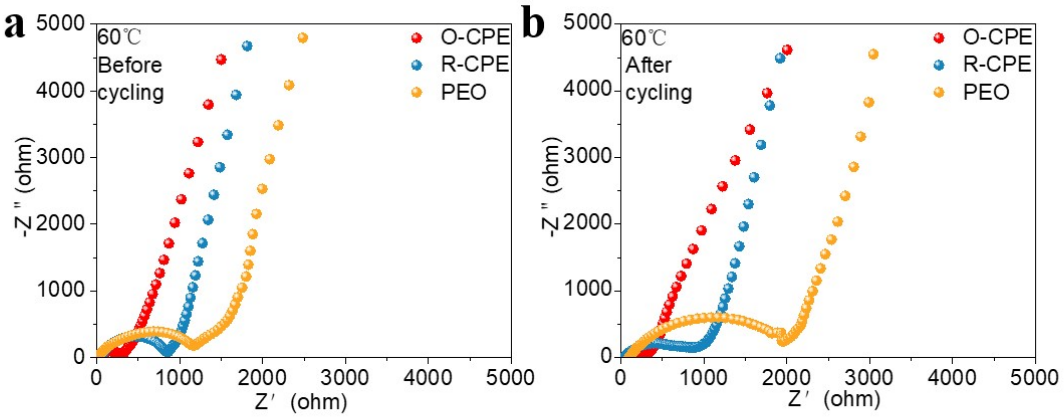

Fig. S20. EIS curves of different electrolyte films in LFP-based cells (a) before and (b) after long-term cycling at 1C and 60 °C.

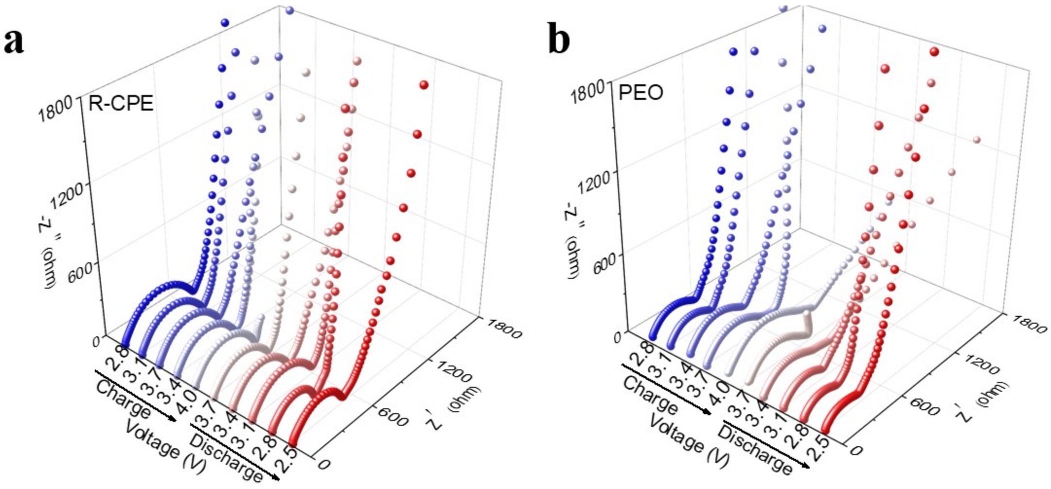

Fig. S21. In situ EIS during charging process and discharging process of (a) LFP/R-CPE/Li and (b) LFP/PEO /Li cells.

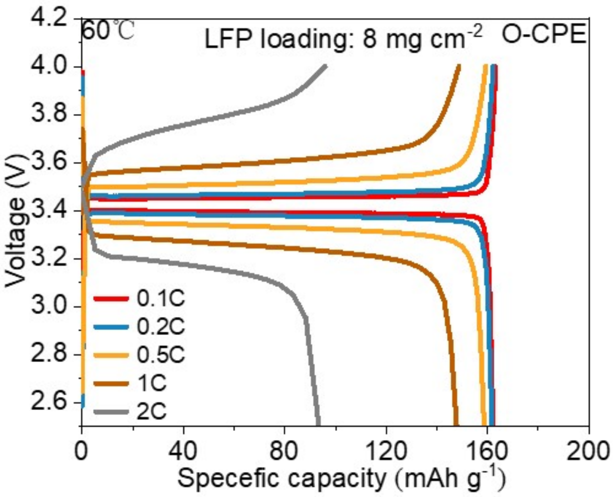

Fig. S22. Corresponding voltage curves of high LFP loading (8.0 mg cm^{-2}) cell with O-CPE film under different rates at 60 °C.

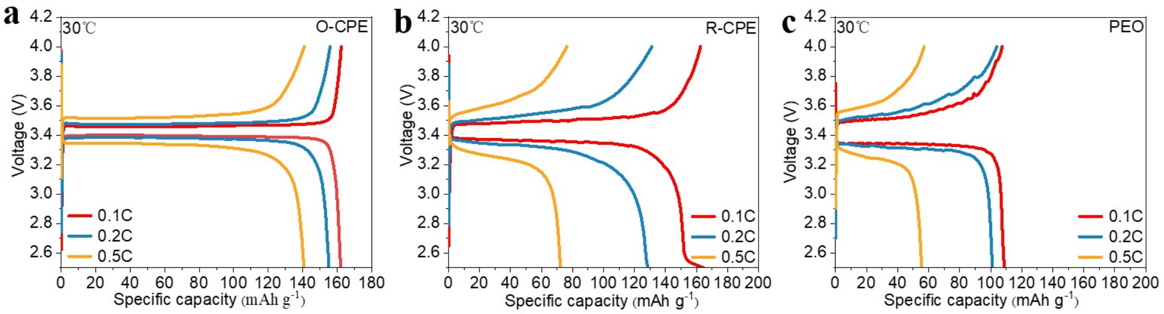

Fig. S23. Corresponding voltage curves of (a) O-CPE, (b) R-CPE and (c) PEO full cells under different rates at 30 °C.

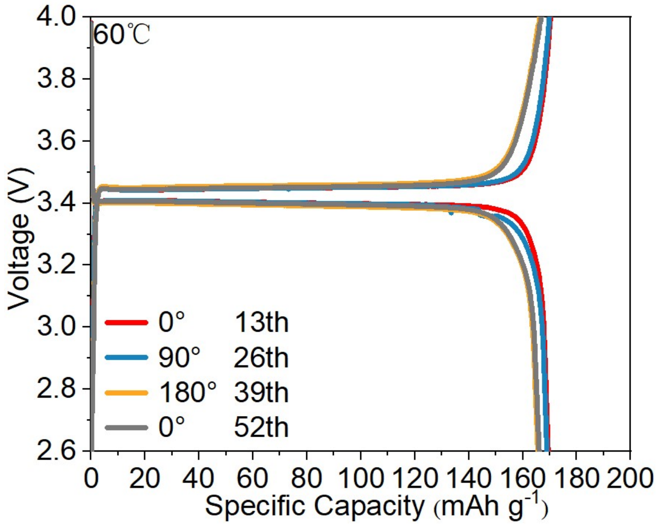

Fig. S24. Voltage profiles of the LFP/O-CPE/Li pouch cell at various bending degrees.

Table S1. COMSOL Multiphysics simulation related parameters.

Solid electrolytes	O-CPE	R-CPE	PEO
Electrolyte conductivities (S cm^{-1})	8.9×10^{-4}	4.24×10^{-4}	2.4×10^{-4}
D_{Li^+} (cm^2 s^{-1})	16.03×10^{-12}	8.13×10^{-12}	1×10^{-12}
D_{TFSI^-}(cm^2 s^{-1})	11.61×10^{-12}	7.87×10^{-12}	3.35×10-12
Nanocrystals length (um)	20	20	-
Nanocrystals angles (°)	0	10-50	-
Charging rate (C)	0.1	0.1	0.1

Table S2. Comparison of the LFP loading and the areal capacity with previously reported ASSLBs.

Solid electrolytes	LFP loading (mg cm^{-2})	Areal capacity (mAh cm^{-2})	Ref.
O-CPE	8	1.31	This work
PVDF-HFP-Li7La3Zr2O12+LE	2.26	0.31	S[1]
LAGP-80	3.6	0.5	S[2]
PEO-0.5LLZTO	1	0.14	S[3]
PCL/SN-SPE	1.9	0.27	S[4]
CSSE	3	0.45	S[5]
PI/PEO	6.9	0.9	S[6]
PPL	7	0.94	S[7]
LLZO/PEO	4.7	0.73	S[8]
ZnO@LATP	2.55	0.41	S[9]

Table S3. Comparison with solid electrolytes reported in the literature (Under 60 °C).

Solid electrolytes	Cycle life (h)	σ (mS cm^{-1})	t_{Li}^{+}	ESW (V)	Rate performance (C)	Ref.
O-CPE	3200	0.89	0.58	4.97	10	This work
LP/CN@B-NBC	2100	0.784	0.64	5.1	1	S[10]
PEO/LiTFSI/3%BC	1160	0.784	0.57	4.98	2	S[11]
PEO-TiO_2(B)	2350	0.66	0.4	5	2	S[12]
PEO16+2%GF@HCS	600	0.44	0.18	3.9	4	S[13]
PEO/L-5Z	950	0.294	0.204	5	2	S[14]
PEO/GO-PSLi	1100	0.22	0.53	4.3	4	S[15]
PL/10HM	240	0.9	0.38	4.71	1	S[16]
MOF808@PAN @PEO-LiTFSI	1800	0.407	0.42	5.3	1	S[17]
PLP-10%LLZVO	1800	1	0.84	4.86	5	S[18]

Supplementary References

1. Y. F. Liang, S. J. Deng, Y. Xia, X. L. Wang, X. H. Xia, J. B. Wu, C. D. Gu and J. P. Tu, *Mater. Res. Bull.*, 2018, **102**, 412-417.
2. Y.-C. Jung, S.-M. Lee, J.-H. Choi, S. S. Jang and D.-W. Kim, *J. Electrochem. Soc.*, 2015, **162**, A704.
3. S. H.-S. Cheng, K.-Q. He, Y. Liu, J.-W. Zha, M. Kamruzzaman, R. L.-W. Ma, Z.-M. Dang, R. K. Y. Li and C. Y. Chung, *Electrochim. Acta*, 2017, **253**, 430-438.
4. D. Zhang, L. Zhang, K. Yang, H. Wang, C. Yu, D. Xu, B. Xu and L.-M. Wang, *ACS Appl. Mater. Interfaces*, 2017, **9**, 36886-36896.
5. P. Zhai, L. Fu, S. Yuan, L. Shi, J. Zhu, Y. Zhao and Z. Wang, *ACS Appl. Energy Mater.*, 2020, **3**, 7011-7019.
6. J. Wan, J. Xie, X. Kong, Z. Liu, K. Liu, F. Shi, A. Pei, H. Chen, W. Chen, J. Chen, X. Zhang, L. Zong, J. Wang, L.-Q. Chen, J. Qin and Y. Cui, *Nat. Nanotechnol.*, 2019, **14**, 705-711.
7. J. Wu, Z. Rao, Z. Cheng, L. Yuan, Z. Li and Y. Huang, *Adv. Energy Mater.*, 2019, **9**, 1902767.
8. C.-Z. Zhao, X.-Q. Zhang, X.-B. Cheng, R. Zhang, R. Xu, P.-Y. Chen, H.-J. Peng, J.-Q. Huang and Q. Zhang, *Proc. Natl. Acad. Sci.*, 2017, **114**, 11069-11074.
9. X. Hao, Q. Zhao, S. Su, S. Zhang, J. Ma, L. Shen, Q. Yu, L. Zhao, Y. Liu, F. Kang and Y.-B. He, *Adv. Energy Mater.*, 2019, **9**, 1901604.
10. S. Yin, Y. Huang, Y. Liu, L. Cheng, M. Chen, Y. Xu, F. Seidi and H. Xiao, *Adv. Funct. Mater.*, 2024, **34**, 2314976.
11. Y. Li, Z. Sun, D. Liu, S. Lu, F. Li, G. Gao, M. Zhu, M. Li, Y. Zhang, H. Bu, Z. Jia and S. Ding, *Energy Environ. Mater.*, 2021, **4**, 434-443.
12. J. Li, Y. Cai, F. Zhang, Y. Cui, W. Fang, H. Da, H. Zhang and S. Zhang, *Nano Energy*, 2023, **118**, 108985.
13. X. Wang, X. Shen, P. Zhang, A.-J. Zhou and J.-B. Zhao, *Rare Metals*, 2023, **42**, 875-884.
14. C. Li, S. Deng, W. Feng, Y. Cao, J. Bai, X. Tian, Y. Dong and F. Xia, *Small*, 2023, **19**, 2300066.
15. Z. Hu, W. Bao, Y. Zhang, X. Jiang, J. Chen, Y. Zhang, S. Huo, J. Zhang, J. Qin, S. Li, W.

Guo and H. Cheng, *Chem. Eng. J.*, 2023, **472**, 144932.

16. C.-C. Sun, A. Yusuf, S.-W. Li, X.-L. Qi, Y. Ma and D.-Y. Wang, *Chem. Eng. J.*, 2021, **414**, 128702.
17. M. Xu, S. Liang, H. Shi, J. Miao, F. Tian, W. Cui, R. Shao and Z. Xu, *Small*, 2024, **20**, 2406007.
18. Y. Li, D. Han, X. Gao, J. Shi, W. Wang, H. Wang and L. Zheng, *Chem. Eng. J.*, 2024, **496**, 154259.